APL Materials

Structural and electronic properties of $SrCuO_{2+\delta}$ thin films

Cite as: APL Mater. **10**, 101112 (2022); https://doi.org/10.1063/5.0107320
Submitted: 04 July 2022 • Accepted: 22 September 2022 • Published Online: 31 October 2022

Marios Hadjimichael, Adrien Waelchli, Bernat Mundet, et al.

Structural and electronic properties of $SrCuO_{2+\delta}$ thin films

Cite as: APL Mater. 10, 101112 (2022); doi: 10.1063/5.0107320
Submitted: 4 July 2022 • Accepted: 22 September 2022 •
Published Online: 31 October 2022

Marios Hadjimichael,[1,a)] Adrien Waelchli,[1] Bernat Mundet,[1,2] Siobhan McKeown Walker,[1,3] Gabriele De Luca,[4] Javier Herrero-Martín,[5] Marta Gibert,[6] Stefano Gariglio,[1] and Jean-Marc Triscone[1]

AFFILIATIONS

[1] Department of Quantum Matter Physics, University of Geneva, 24 Quai Ernest-Ansermet, 1211 Geneva, Switzerland
[2] Electron Spectrometry and Microscopy Laboratory, Institute of Physics, École Polytechnique Fédérale de Lausanne, 1015 Lausanne, Switzerland
[3] Laboratory of Advanced Technology (LTA), 24 Quai Ernest-Ansermet, 1211 Geneva, Switzerland
[4] Catalan Institute of Nanoscience and Nanotechnology (ICN2), Bellaterra, Barcelona, Spain
[5] ALBA Synchrotron Light Source, Carrer de la Llum 2-26, 08290 Cerdanyola del Vallès, Spain
[6] Solid State Physics Institute, TU Wien, Wiedner Hauptstr. 8-10/138, 1040 Vienna, Austria

[a)] **Author to whom correspondence should be addressed:** marios.hadjimichael@unige.ch

ABSTRACT

The layered structure of superconducting cuprates is considered to be a key ingredient to achieve high superconducting transition temperatures. In this work, we investigate the possibility of doping the $SrCuO_2$ infinite-layer compound by inserting additional oxygen into its structure. We observe that the infinite-layer $SrCuO_2$ structure is epitaxially stabilized in thin films grown by pulsed laser deposition in pure O_2. Increasing the oxidizing power by introducing ozone during the growth leads to a different phase with an elongated *c* axis. Scanning transmission electron microscopy analysis suggests that the films with an elongated *c* axis are composed of $SrCuO_{2.5}$ blocks separated by $SrCuO_2$ layers arranged to match the substrate spacing. X-ray absorption spectroscopy measurements show that this $SrCuO_{2+\delta}$ phase is associated with a more isotropic Cu orbital configuration and hole doping. This hole doping leads to a dramatic reduction in the resistivity of the films, with a magnitude that depends on the precise oxygen content in the structure.

I. INTRODUCTION

The crystal structure of superconducting cuprates[1] is characterized by a layered arrangement of CuO_2 atomic planes separated by planes of cations; a charge-transfer mechanism between these planes provides the charge carriers that lead to electrical conduction.[2] In its simplest form, where the ordering of planes is a regular alternation of CuO_2 planes and atomic *A* planes (*A* usually being an alkaline metal), the structure is called infinite layer and has received considerable attention for its key role in the mechanism of superconductivity.[3] Additionally, the recent discovery of superconductivity in nickel compounds with the same infinite-layer structure[4] has reignited interest in the $ACuO_2$ phases, whose synthesis has always been challenging. The synthesis of superconducting nickelates requires a reduction of the oxygen content from the perovskite $RNiO_3$ phase (*R* being La, Pr, or Nd) to the infinite-layer $RNiO_2$ via a soft chemical route.[5–10] In contrast, the cuprates can be synthesized directly in the infinite-layer structure. In the bulk form, however, they require extreme conditions of temperature and pressure,[11–13] while epitaxy enables their growth as crystalline layers in thin film form.[14–16]

Achieving superconductivity in the infinite-layer cuprates is a difficult task: when the separating cation is an alkaline metal ($CaCuO_2$, $SrCuO_2$, or $BaCuO_2$), Cu is in a 2+ valence state and the compounds are antiferromagnetic insulators; they can be made superconducting through electron doping, by replacing the divalent alkaline metal with a trivalent lanthanide.[11,17,18] In hole doped systems, cation vacancies or interstitial oxygen atoms, apical to the Cu, have been reported as effective mechanisms to induce superconducting transitions.[19] Superlattices of $BaCuO_2/SrCuO_2$[20,21] and

$BaCuO_2/CaCuO_2$[22,23] have superconducting critical temperatures as high as 70 K, attributed to the doping effect of apical oxygen inserted into the Ba planes. More recently, the proximity of a perovskite phase to the infinite-layer structure in $SrTiO_3/CaCuO_2$ bilayers and superlattices has been shown to be another heterostructuring approach to observe superconductivity via the introduction of apical oxygen.[24,25] These studies have demonstrated that precise manipulation of the oxygen content and the arrangement of oxygen atoms in infinite-layer cuprates is crucial to engineer their electronic properties.

In this work, we show that control of the oxygen configuration in infinite-layer cuprate thin films can be achieved by tuning the oxidizing power during film growth using ozone-assisted pulsed laser deposition. The oxidizing power can be varied by fixing the O_3/O_2 percentage and varying the gas mixture flow during the growth of $SrCuO_{2+\delta}$ films. As the oxidizing power is increased, we find that a different phase with an elongated c axis appears ($SrCuO_{2+\delta}$): the macroscopic phase fraction of $SrCuO_{2+\delta}$ and $SrCuO_2$ can be controlled precisely with the O_3/O_2 flow. With reference to previous experimental and theoretical work, we discuss the possible structures and oxygen content values of the high c-axis $SrCuO_{2+\delta}$ phase.

Planar-view aberration-corrected scanning transmission electron microscopy (STEM) measurements show that the $SrCuO_{2+\delta}$ thin films are characterized by a modulation of the in-plane spacing between consecutive Sr atoms. Regions with expanded in-plane lattice parameter appear as dark stripes along either the [100] or the [010] direction in Z-contrast images and arise due to the ordering of oxygen vacancies (with respect to the stoichiometric $SrCuO_{2.5}$ structure) along one of the two crystallographic axes when δ is smaller than 0.5. Using x-ray absorption spectroscopy (XAS), we show that this high c-axis $SrCuO_{2+\delta}$ phase is associated with a more isotropic orbital coordination for Cu compared to the infinite-layer structure, as well as with hole doping. Transport measurements as a function of temperature reveal that this hole doping leads to a dramatic decrease in the resistivity, with a magnitude that depends on the precise oxygen content of the structure.

II. EXPERIMENTAL

$SrCuO_{2+\delta}$ thin films were deposited on (001)-oriented $SrTiO_3$ substrates (Crystec GmbH) using pulsed laser deposition with a KrF excimer laser (248 nm, 25 ns) by ablating from a stoichiometric ceramic target (Praxair Surface Technologies). The films were grown at a constant pressure of 0.25–0.5 mbar, in a pure oxygen (O_2) atmosphere, or in a mixture of oxygen and ozone (O_2 + 5% O_3). The gas mixture was delivered into the chamber through a stainless steel tube pointing toward the substrate and placed 3–4 cm away from it. The oxidizing power during the growth was varied by controlling the flow through the tube using a flow meter, with O_2 + O_3 flows ranging from 10 to 20 standard cubic centimeters per minute (sccm). During growth, the substrate was kept at a constant temperature of 600 °C, heated using an infrared laser. Following deposition, the samples were quenched to room temperature in the same atmosphere used during the growth.

Structural characterization of the $SrCuO_{2+\delta}$ thin films was conducted using a PANalytical X'Pert Pro diffractometer with a Cu $K\alpha$ source. STEM measurements were used to get information on the local structure of the films using a double-corrected Thermofisher TITAN Themis electron microscope, equipped with a double-corrector DCOR (CEOS) and a high brightness field emission gun with monochromator, operated at 300 kV in STEM mode using a semi-convergence angle of 20 mrad. The monochromator allowed us to acquire the data using low beam currents (around 30–40 pA), ensuring no beam damage. To improve the image quality and reduce scanning distortions, we acquire stacks of images that are then cross-correlated using the SmartAlign plug-in for DigitalMicrograph.[26] The TEM specimen was prepared following mechanical polishing and an ion milling process (carried out at a temperature of −100 °C to minimize sample damage) to thin the specimen down to electron transparency. The coordinates associated with each Sr column have been estimated using a 2D Gaussian fitting procedure using the Atomap script.[27]

XAS was used to determine the orbital configuration of the thin films. XAS measurements were performed in total electron yield mode across the oxygen K and copper $L_{2,3}$ edges in the BL29-BOREAS beamline[28] of the ALBA Synchrotron (Barcelona, Spain) at room temperature, under ultra-high vacuum conditions (2×10^{-10} mbar). The photon flux on the samples was $\sim 10^{12}$ photons/s with an energy resolution of 50 meV at the O K edge and about 120 meV at the Cu L_3 edge. Low-temperature resistivity measurements were performed using a probe slowly dipped in liquid helium as well as an Oxford Instruments Teslatron low-temperature system. For both types of measurements, a current of 1–100 μA was supplied using a Keithley 224 or 622X Current Source, and a voltage was measured in four-point van der Pauw geometry using a Keithley 2000 Multimeter or a Keithley 2182 A Nanovoltmeter, with the four corners of the sample contacted using Al wire-bonding.

III. RESULTS

A. Structural characterization

Figure 1(a) shows large-range θ-2θ scans around the 001 and 002 peaks of $SrTiO_3$ for $SrCuO_{2+\delta}$ thin films with a thickness of ~20 nm (50–59 unit cells). The film deposited in oxygen (bottom curve, blue) shows finite-size oscillations around the 00L reflections, which correspond to the tetragonal infinite-layer phase with an out-of-plane lattice parameter of c = 3.45 Å. The oxidizing power during the growth has been progressively increased by introducing ozone into the chamber (using a mixture of O_2 + 5% of O_3) and raising the flow rate from 10 to 20 sccm. At 15 sccm, an additional Bragg peak appears, associated with an out-of-plane lattice parameter of 3.64 Å. Further increasing the flow rate of the oxygen/ozone mixture (20 sccm), we observe that only the high c-axis peak remains while its position moves slightly to lower 2θ values. Multiple samples of the high c-axis phase were deposited at this high O_2/O_3 mixture flow, for which we found a variation in their out-of-plane lattice parameter that ranges from 3.63 to 3.71 Å. The variation in lattice parameters indicates a range of oxygen contents in these films, as will be discussed below. We note that the jump in the c axis when ozone is introduced into the chamber indicates that the additional oxygen is not gradually incorporated into the structure, but rather that a new phase occurs. Despite the large change in the lattice parameter from the infinite-layer to this high c-axis phase (~6% increase), both structures remain strained to the $SrTiO_3$ substrate as seen in the reciprocal space maps around the $\bar{1}03$ peak of

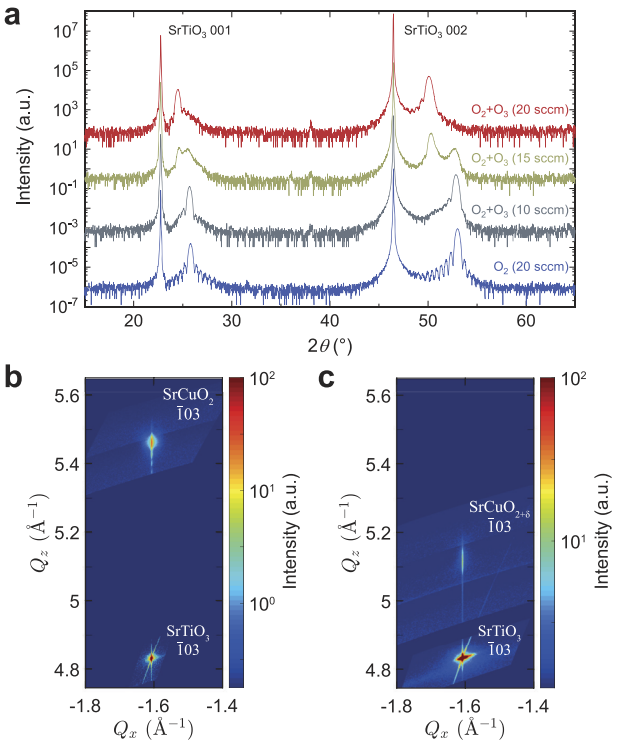

FIG. 1. Structural characterization of $SrCuO_{2+\delta}$ thin films. (a) θ-2θ scan of a series of $SrCuO_{2+\delta}$ films deposited under varying oxidizing growth conditions. Bottom curve: Film deposited in pure oxygen. Top curves: Films deposited in an ozone/oxygen atmosphere with an ozone percentage of 5%, where the oxidizing power is progressively increased by increasing the flow rate from 10 to 20 sccm. A clear redistribution of intensity between two Bragg peaks is observed, with the 002 infinite-layer peak at 2θ = 52.97°(c = 3.45 Å), and the high c-axis peak at 2θ = 50.13°(c = 3.64 Å). The peak at 2θ = 38.0°comes from the diffractometer sample holder. (b) and (c) Reciprocal space maps around the $\bar{1}03$ peak of the $SrTiO_3$ substrate for the sample deposited in pure oxygen and in 20 sccm of O_2 + O_3, respectively, showing that despite the large change in out-of-plane lattice parameter both films remain strained to the substrate.

$SrTiO_3$ [Figs. 1(b) and 1(c)]. Additionally, the reciprocal space map around the $0\bar{1}3$ peak of $SrTiO_3$ for the high c-axis phase (not shown here) is identical to Fig. 1(c), indicating that no in-plane asymmetry occurs.

To determine the structure that can give rise to this larger out-of-plane lattice parameter, we have to consider all possible phases of $SrCuO_2$, $SrCuO_{2+\delta}$ and $Sr_{n+1}Cu_nO_{2n+1}$. First, in addition to the tetragonal structure, $SrCuO_2$ can crystallize in an orthorhombic phase[29] when deposited at very high temperatures.[30,31] This structure would give rise to a very large change in the unit cell size, with c = 16.311 Å, leading to additional diffraction peaks. We observe this phase only when we deposit $SrCuO_2$ in pure oxygen at temperatures higher than 650 °C, as shown in the supplementary material Fig. S1, showing diffraction signatures that are distinct from the observed elongated c-axis phase in Fig. 1(a).

Second, a chain-type $SrCuO_2$ structure with a c axis of 3.9 Å was previously reported when the thickness of $SrCuO_2$ is reduced to below approximately five unit cells.[32–34] This structure results from a rotation of the CuO_2 planes by 90°. Our films are much thicker than this, and our observed c-axis value is smaller.

Additionally, phases in the $Sr_{n+1}Cu_nO_{2n+1}$ system can be easily excluded because they have larger lattice parameters than those we observe: the n = 1 phase (Sr_2CuO_3) would already show additional diffraction peaks corresponding to an out-of-plane lattice parameter of 12.548 Å.[35–37] These phases would also change the Sr/Cu stoichiometry very drastically, not something we expect simply by introducing ozone into the system.

Finally, an elongated out-of-plane lattice parameter has previously been observed in $SrCuO_{2+\delta}$ when deposited or post-annealed under highly oxidizing growth conditions,[38–41] or when electron doped using La or Nd substitution.[42–44] This phase was attributed to the incorporation of additional oxygen atoms in the Sr planes, leading to a $SrCuO_{2+\delta}$ structure. In thin films with two distinct Bragg peaks (arising from the infinite-layer and high c-axis structures), a macroscopic phase separation was also previously observed.[44] In Ref. 39, the authors used transmission electron microscopy to characterize the high c-axis phase in Na-doped $Ca_{1-x}Sr_xCuO_{2+\delta}$ thin films and have found evidence for a $2\sqrt{2}a_p \times 2\sqrt{2}a_p$ superstructure (where a_p is the in-plane lattice parameter of the $SrTiO_3$ substrate), leading them to determine a value of δ = 0.25. Nevertheless, due to the extreme sensitivity of the samples to the measurement conditions and their fast degradation, the origin of this superstructure and the precise oxygen content of the high c-axis phase could not be confirmed.

Seko and Ishiwata,[45] using density functional theory and Bayesian optimization, determined the most stable $SrCuO_{2+\delta}$ structures for various values of δ. Out of the calculated lowest energy structures, only two have been observed experimentally: these are the structures with the two extreme values of δ equal to 0 and 0.5. For δ = 0 ($SrCuO_2$), the most stable structure is the infinite-layer with tetragonal unit cell lattice parameters $a_t = b_t$ = 3.927 Å, c_t = 3.435 Å [shown in Figs. 2(a)–2(c)].[46] For δ = 0.5, the most stable structure is one consisting of corner-sharing CuO_5 pyramids [shown in Figs. 2(d) and 2(e)] that has been observed when $SrCuO_{2.5}$ is prepared at 950 °C and a pressure of 100 kbar.[47] This phase has a similar structure to $CaMnO_{2.5}$[48] and $LaCuO_{2.5}$,[49] and has an orthorhombic unit cell, with a_o = 5.424 Å, b_o = 10.837 Å, c_o = 3.731 Å. The $SrCuO_{2.5}$ structure can be represented using a pseudocubic unit cell as shown in red in Fig. 2(d), with $a_p = a_o/\sqrt{2}$ = 3.835 Å, $b_p = b_o/(2\sqrt{2})$ = 3.831 Å, $c_p = c_o$ = 3.731 Å.[47] We note that, in contrast to the infinite-layer $SrCuO_2$ structure, the $SrCuO_{2.5}$ phase does not exhibit continuous CuO_2 planes in the in-plane a_p and b_p directions.

Two other structures have been predicted depending on the precise oxygen content in $SrCuO_{2+\delta}$. For δ = 0.375, a structure with local CuO_6 octahedra, CuO_5 pyramids, and CuO_4 squares that are parallel or perpendicular to the c axis, is predicted, shown in the supplementary material Fig. S2. This structure has a tetragonal unit cell with $a = b$ = 10.6056 and c = 3.7362 Å.[45] For δ = 0.25, a similar tetragonal structure is predicted, with $a = b$ = 10.6212 and c = 3.6919 Å,[45] shown in the supplementary material Fig. S2. For both of these phases, a pseudocubic unit cell can be defined with $a_p = b_p = a_t/2\sqrt{2}$ = 3.755 and 3.750 Å, respectively. Both the $SrCuO_{2.375}$ and $SrCuO_{2.25}$ phases are consistent with the $2\sqrt{2}a_p \times 2\sqrt{2}a_p$ superstructure observed by Wen *et al.* using

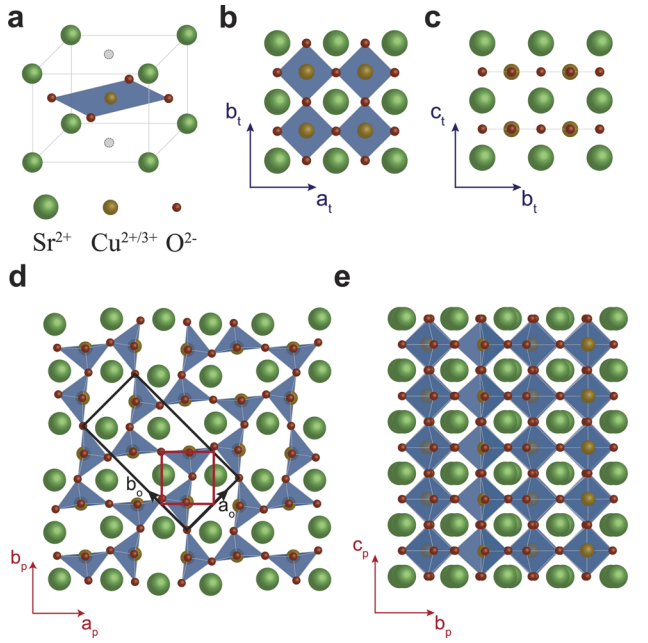

FIG. 2. Schematics of the structures of $SrCuO_{2+\delta}$ for the two extreme values of δ, 0 and 0.5. (a) Perspective view of the infinite-layer $SrCuO_2$ structure. Shown in light gray are the missing oxygen atoms with respect to the ideal perovskite structure, and in blue are the CuO_4 squares. (b) and (c) Schematics of the $SrCuO_2$ structure viewed along the tetragonal *c* and *a* axes, respectively. (d) and (e) Schematics of the $SrCuO_{2.5}$ structure with corner-shared CuO_5 pyramids viewed along the pseudocubic *c* and *a* axes, respectively, as observed experimentally by Chen *et al.*[47] The black rectangle is a sketch of the orthorhombic unit cell with in-plane lattice parameters a_o and b_o. The red square indicates the equivalent pseudocubic unit cell.

transmission electron microscopy.[39] However, the two phases have not been observed in bulk samples so far.

The common feature in all the possible structures of $SrCuO_{2+\delta}$ is the incorporation of oxygen in the Sr planes that are parallel to the interface with the substrate. The incorporation of additional oxygen in our high *c*-axis structure is confirmed by *in situ* x-ray diffraction measurements performed while annealing a $SrCuO_{2+\delta}$ sample in a N_2 atmosphere (see Fig. S3 in the supplementary material).

We would expect to see additional peaks in x-ray diffraction either for the orthorhombic $SrCuO_{2.5}$ or for the larger unit cell of the tetragonal $SrCuO_{2.375}$ or $SrCuO_{2.25}$ structures that originate from the displacements of the Sr and Cu ions from their positions in the infinite layer phase. Using our laboratory diffractometer, however, we have only observed peaks related to the infinite layer structure. We attribute this to the low intensity of the bulk orthorhombic peaks compared to the infinite layer reflections,[47] as well as the possible formation of domains with local oxygen ordering that suppress the intensity of the reflections that originate from a long-range order of the additional oxygen.

To investigate the local structure of the films, we use STEM. Figure 3(a) is a planar-view (viewing axis along the growth direction) high-angle annular dark field (HAADF) image of a $SrCuO_{2+\delta}$ thin film deposited on $SrTiO_3$ with c = 3.626 Å and a thickness equal to 85 unit cells. Due to the Z-contrast nature of the HAADF imaging mode, the brightest spots in the image are Sr atoms, while the second brightest spots are Cu atoms. We find that a modulation of the HAADF contrast appears, with domains of dark stripes aligned along either the [100] or [010] crystallographic axes of the substrate, as indicated by the green and red arrows, respectively. These stripes are generally regularly spaced and lead to the appearance of a superstructure with an in-plane lattice parameter that is on average three times that of $SrTiO_3$, as observed by the additional spots—marked by the corresponding arrows—in the Fourier transform of the HAADF image [Fig. 3(b)].

Dark stripes similar to the ones in Fig. 3(a) have been observed in STEM studies of cobaltite,[50–52] manganite,[53] and ferrite[54] perovskite thin films, and have been attributed to expanded unit cells that are associated with ordered oxygen vacancies. For example, in the brownmillerite $La_{0.6}Sr_{0.4}MnO_{2.5}$ system, the distance between A-site cations varies from 3.783 to 4.527 Å depending on the local coordination of Mn—tetrahedral or octahedral;[55] $LaCoO_{3-x}$ and $La_{0.5}Sr_{0.5}CoO_{3-x}$ show an alternation of expanded (up to 20%) oxygen-depleted layers with CoO_4 triangular pyramids and of perovskite layers with CoO_6 octahedra.[55]

To detect the in-plane modulation of the $SrCuO_{2+\delta}$ structure, we have mapped the atomic positions of Sr in a smaller region of the sample where the dark stripes run along the [100] direction [Fig. 3(c)]. Figure 3(d) is a plot of the distance between consecutive Sr ions as a function of layer number for both the [100] and [010] directions: along the [100] direction, this spacing remains constant, while along the [010] direction a large variation in the Sr–Sr distance is recorded. In the dark stripe regions, the spacing between consecutive Sr atoms has an average value of 3.98 ± 0.01 Å; in the other regions, it decreases to an average value of 3.87 ± 0.01 Å. We note that since no substrate area is available to be used as a reference for image calibration, we have calibrated the pixel size so that the averaged in-plane lattice parameters match those of the $SrTiO_3$ substrate, in agreement with the reciprocal space maps [Fig. 1(c)].

In the $SrCuO_{2+\delta}$ system, the only experimentally observed configurations for copper are CuO_5 square pyramids (in orthorhombic $SrCuO_{2.5}$[47]) and CuO_4 squares (in tetragonal $SrCuO_2$[46]). Our current STEM measurements indicate that $SrCuO_{2+\delta}$ structures with intermediate values of δ between 0 and 0.5 do not adopt the $SrCuO_{2.375}$ or $SrCuO_{2.25}$ structures. However, they most likely manifest as $SrCuO_{2.5}$ structures periodically interrupted by infinite-layer $SrCuO_2$ planes [shown in the sketch of Fig. 3(c)] that appear to accommodate the oxygen off-stoichiometry and to minimize the tensile strain imposed on $SrCuO_{2.5}$ by the $SrTiO_3$ substrate.

The average oxygen content of the $SrCuO_{2+\delta}$ thin film with c = 3.626 Å can be estimated based on the Fourier transform of Fig. 3(b). Considering the tripling of the in-plane unit cell, we can assume the superstructure consists of two unit cells of $SrCuO_{2.5}$ and one unit cell of $SrCuO_2$, and therefore, δ is evaluated to be equal to 0.33. We expect the spacing between the infinite-layer $SrCuO_2$ planes and their phase fraction compared to $SrCuO_{2.5}$ to depend not only on the value of the epitaxial strain but also on the precise oxygen content of the $SrCuO_{2+\delta}$ structure. Therefore, the average out-of-plane lattice parameter of the high *c*-axis $SrCuO_{2+\delta}$ phase

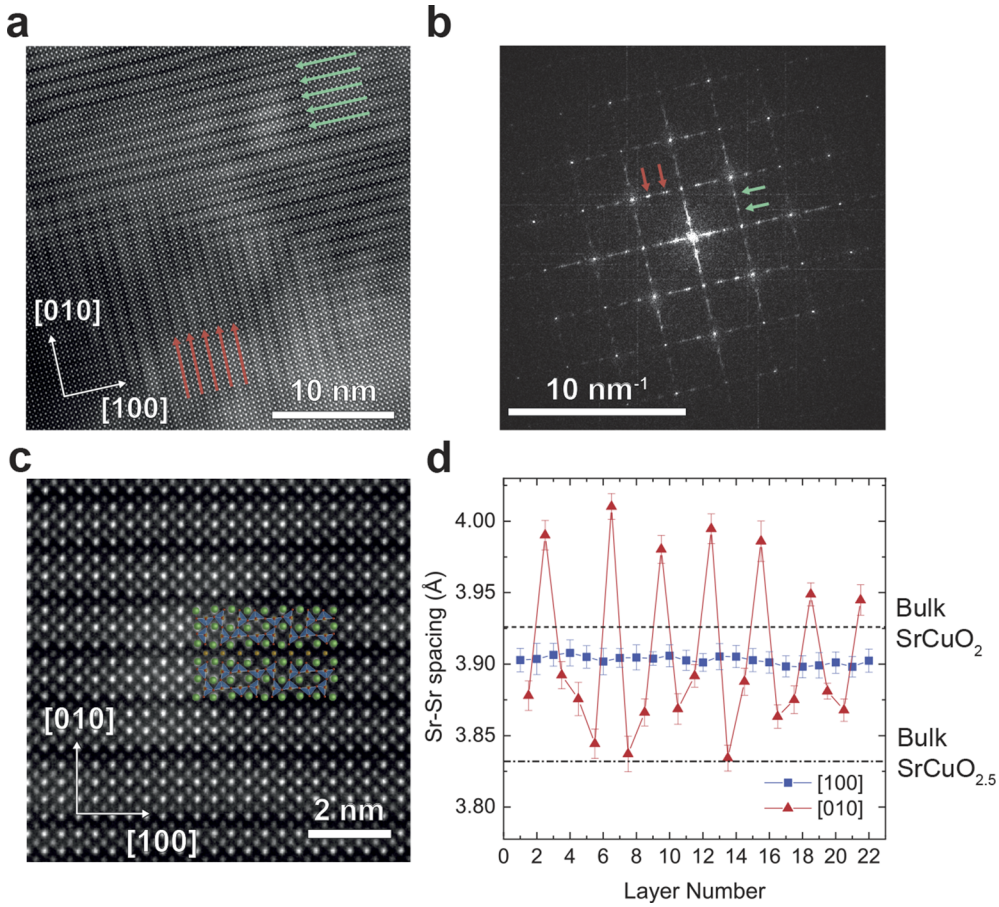

FIG. 3. STEM measurements of a $SrCuO_{2+\delta}$ thin film deposited on $SrTiO_3$, with c = 3.626 Å and a thickness equal to 85 unit cells. (a) Planar-view HAADF image of the film. The white arrows show the directions of the [100] and [010] crystallographic axes of the substrate. Separate domains with dark stripes (regions with a larger Sr–Sr spacing) oriented along [100] or [010] can be observed, marked by green and red arrows, respectively. (b) Fourier transform of the HAADF image in (a), showing that a superstructure appears due to a new unit cell that is on average triple the perovskite cell along either the [100] or the [010] directions. The superstructure peaks corresponding to each domain in (a) are marked by arrows of the same color. (c) HAADF image of a smaller region of panel (a) used to map the interatomic distances between Sr atoms. The schematics show the expected structures—bright regions are expected to be $SrCuO_{2.5}$ unit cells, whereas the darker stripes with expanded in-plane lattice parameter are expected to be infinite-layer $SrCuO_2$. We note that as the positions of oxygen atoms are not known from the STEM measurements, the schematics are based on the bulk $SrCuO_{2.5}$ structure. The precise oxygen connectivity between $SrCuO_{2.5}$ and $SrCuO_2$ phases is not known and, therefore, not shown here. (d) Interatomic distances between Sr atoms extracted from the HAADF image in (c) along [100] (blue squares) and [010] (red triangles). Each value is obtained from the mean Sr–Sr spacing of two consecutive atomic rows/columns (for [010] and [100], respectively) and the error bars correspond to the standard error in the mean. The distances between Sr atoms in the [100] direction remain constant, while a periodic expansion occurs in the [010] direction.

should give an indication of the precise oxygen content, with a higher c-axis value indicating a larger value of δ, due to a smaller fraction of infinite-layer $SrCuO_2$ planes in the structure. Finally, we note that the periodic insertion of an infinite layer unit cell breaks the long range order of the oxygen in the $SrCuO_{2.5}$ regions, which explains the absence of orthorhombic peaks in x-ray diffraction measurements.

B. Electronic properties of $SrCuO_2$ and $SrCuO_{2+\delta}$ films

To understand the electronic properties of the $SrCuO_{2+\delta}$ system and its differences from the infinite-layer $SrCuO_2$ structure, we use XAS. Figure 4(a) displays a schematic of the measurement geometry: linear vertical (LV) and linear horizontal (LH) polarisations result in the electric field of the incident X rays having a purely in-plane (I_{ab}) or majority out-of-plane (I_c) component, respectively. Figure 4(b) is a plot of the Cu $L_{2,3}$ XAS spectra measured for two orthogonal light polarization directions for an infinite-layer $SrCuO_2$ thin film deposited on $SrTiO_3$ (c = 3.460 Å, thickness = 39 unit cells). The peaks at the L_2 and L_3 edges correspond to transitions from Cu $2p_{1/2}$ to Cu $3d$ and from Cu $2p_{3/2}$ to Cu $3d$ orbitals, and occur at ~952 and 932 eV, respectively. For an undoped infinite-layer structure, the predominant transitions are labeled $2p^63d^9 \rightarrow 2p^53d^{10}$.[4,56–62]

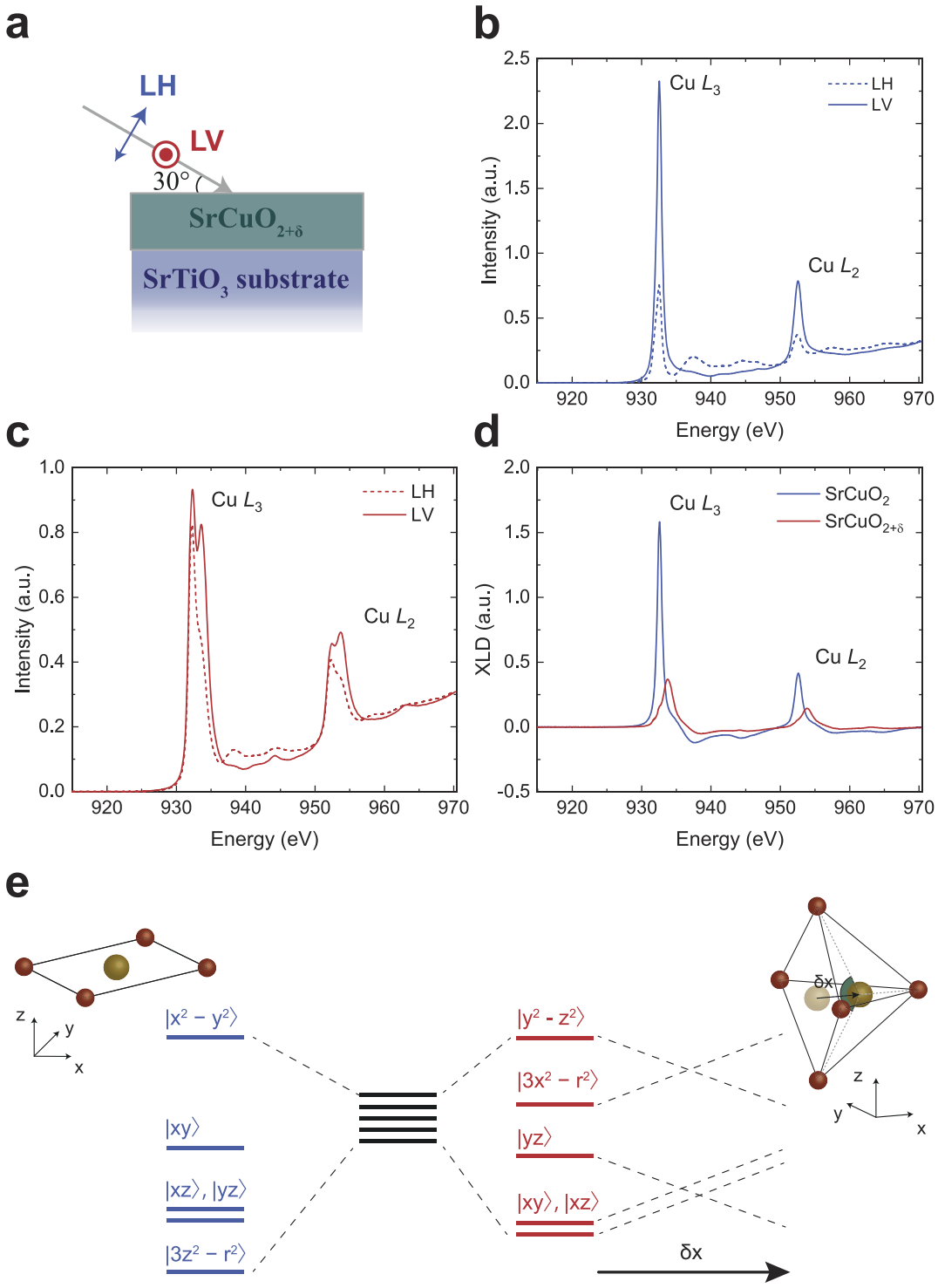

FIG. 4. Orbital polarization observed using grazing incidence x-ray absorption spectroscopy. (a) Schematic of the measurement geometry. LH stands for linear horizontal (I_c) and LV for linear vertical (I_{ab}) polarisations of the incident beam. X-ray absorption spectra around the Cu $L_{2,3}$ edges for LH and LV polarisations for (b) the infinite-layer $SrCuO_2$ phase and (c) the high *c*-axis $SrCuO_{2+\delta}$ phase. (d) X-ray linear dichroism (XLD) calculated by the difference in LH and LV intensities (XLD = $I_{ab} - I_c$) around the Cu $L_{2,3}$ edges. The equivalent O *K* edge spectra are presented in Fig. S4 in the supplementary material. (e) Schematic of the energy splitting of Cu 3*d* orbitals for a CuO_4 square (left) and a CuO_5 pyramid as a function of the displacement of Cu perpendicular to the basal plane, δx, inside the pyramid (right). The O–Cu–O bond angle (shaded in green) adopts values lower than 180° for finite δx.

The absorption intensity in XAS is proportional to the number of unoccupied electronic orbitals coupling to the polarization of the incoming light. Thus, the dramatically lower Cu $L_{2,3}$ peak intensities seen in Fig. 4(b) for LH polarization indicate that the occupation of the out-of-plane electronic orbitals [$3d_{3z^2-r^2}$ and $3d_{xz}(3d_{yz})$] is much higher than the in-plane ones ($3d_{x^2-y^2}$ and $3d_{xy}$). This agrees with the orbital configuration expected for Cu in planar tetrahedral coordination where the in-plane orbitals are pushed to higher energy by crystal field effects and are thus unoccupied for Cu 2+ [see Fig. 4(e)], as previously observed in infinite-layer structures.[24,33,63,64]

Figure 4(c) is a plot of the Cu $L_{2,3}$ XAS spectra for the $SrCuO_{2+\delta}$ structure (c = 3.679 Å, thickness = 38 unit cells). In contrast to the spectra for $SrCuO_2$, the difference in intensity between LV and LH is much smaller, indicating that the Cu coordination is more isotropic. The large differences between the $SrCuO_2$ and $SrCuO_{2+\delta}$ orbital configuration can be better appreciated by calculating the x-ray linear dichroism at the Cu $L_{2,3}$ edges (XLD = $I_{ab} - I_c$), plotted in Fig. 4(d). Considering the crystal field for Cu 3d orbitals in a CuO_4 square and in a CuO_5 pyramid (with apex in the in-plane direction), we expect the two orbital configurations sketched in Fig. 4(e). Note that since the apex of the CuO_5 pyramid in Fig. 4(e) is in the x direction, the orbital pointing from Cu to the apical oxygen in the pyramid is $3d_{3x^2-r^2}$. Similarly, for a CuO_5 pyramid with an apex in the y direction, the corresponding orbital is $3d_{3y^2-r^2}$.

For the CuO_5 pyramid sketched in Fig. 4(e), the energy splitting depends on the exact atomic position of Cu and its distance from the basal plane, δx,[65] with the in-plane orbitals ($3d_{3x^2-r^2}$ and $3d_{xy}$) going up in energy for increasing δx. In the experimentally observed structure of $SrCuO_{2.5}$, the average O–Cu–O bond angle is 172.7°,[47] making δx and δy finite, in agreement with our observation of a lower occupation of in-plane orbitals for $SrCuO_{2+\delta}$.

Coincident with the change in the Cu 3d orbital configuration from the infinite-layer $SrCuO_2$ to $SrCuO_{2+\delta}$, we expect a significant degree of hole doping and a change in the formal valence of copper with the incorporation of additional oxygen. To investigate this doping further, we calculate the XAS spectra [XAS = $(I_{ab} + I_c)/2$] for the two structures and plot them in Fig. 5.

First, we focus on the Cu $L_{2,3}$ edges, shown in Fig. 5(a). As mentioned above, in the infinite-layer $SrCuO_2$ structure, two distinct peaks are observed at ~932 and 952 eV, attributed predominantly to $2p^63d^9 \rightarrow 2p^53d^{10}$ transitions. In $SrCuO_{2+\delta}$, additional intensity appears at higher energies for both Cu L_2 and L_3. This contribution is most likely associated with $2p^63d^9\underline{L} \rightarrow 2p^53d^{10}\underline{L}$ transitions, where $\underline{L}$ denotes a hole in the oxygen ligand p-bands and has been observed in various hole-doped cuprates as a function of hole doping.[4,56,59–63,66–68] Increasing hole doping causes an increase in the amplitude of the higher energy peak, making it possible to roughly estimate the concentration of holes per Cu atom, using the formula $p = I_{|3d^9\underline{L}\rangle}/\left(I_{|3d^9\rangle} + I_{|3d^9\underline{L}\rangle}\right)$, where I is the integrated area of each Cu L_3 peak component.[59,61,69] By fitting the Cu L_3 peak with two pseudo Voigt functions to extract $I_{|3d^9\rangle}$ and $I_{|3d^9\underline{L}\rangle}$ (see the supplementary material Fig. S5), we can get an estimate of the hole doping p = 0.6–0.7 (δ = 0.30–0.35), with an uncertainty in the value arising from the choice of background subtraction. However, additional uncertainty in the determination of the hole doping can arise due to the large structural differences between $SrCuO_2$ and $SrCuO_{2+\delta}$ (this uncertainty is discussed further in the supplementary material).

The spectra at the O K edge for the two structures are shown in Fig. 5(b). The pre-edge region (E < 531 eV) of $SrCuO_2$ is

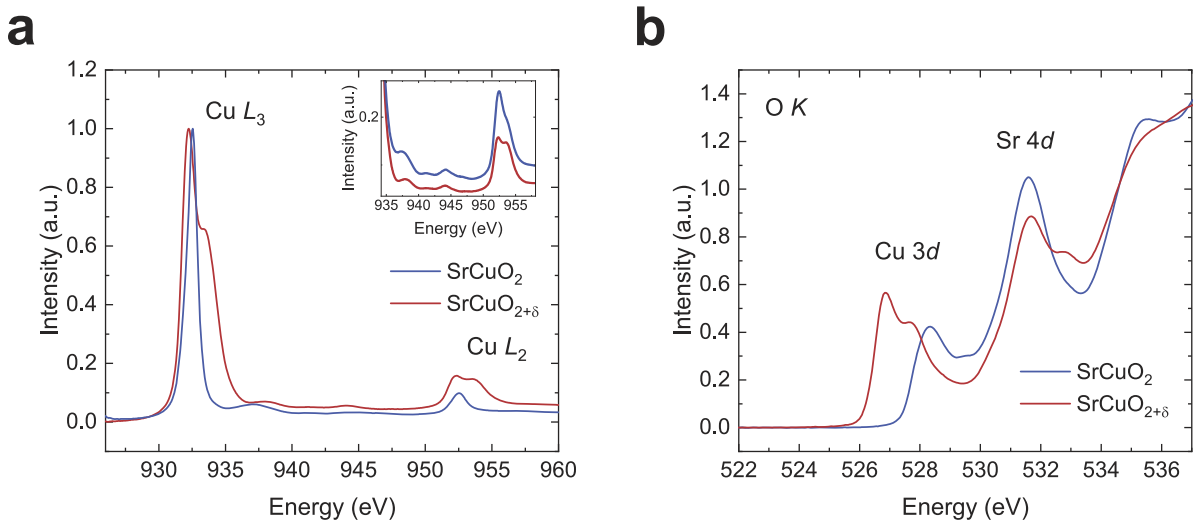

FIG. 5. Hole doping observed using x-ray absorption spectroscopy. Total electron yield absorption spectra around the (a) Cu $L_{2,3}$ edges and (b) O K edge. In (a), the spectrum of the infinite-layer phase (blue) shows a single Cu L_3 peak associated with a predominant transition from a $2p^63d^9$ initial state to a $2p^53d^{10}$ final state. In the high c-axis phase (red), an additional high energy feature associated with a predominant transition from a $2p^63d^9\underline{L}$ initial state to a $2p^53d^{10}\underline{L}$ final state appears. In (b), O K pre-edge peaks appear due to the hybridization with Cu 3d and Sr 4d orbitals. In the high c-axis $SrCuO_{2+\delta}$ phase, a shift of the feature caused by the Cu 3d states to lower energies occurs, concomitant with a change in peak shape that shows new spectroscopic features compared to $SrCuO_2$.

characterized by a single peak at ~528.3 eV, due to a transition to the upper Hubbard band with a Cu 3*d* character hybridized with O 2*p* (referred to as peak U[4]). In $SrCuO_{2+\delta}$, an additional peak appears at lower energies, and peak U shifts to a lower energy. This additional peak can be attributed to two effects. First, this change in the O *K*-pre-edge region may reflect the modification of the crystal structure when additional oxygen atoms are inserted. In other oxide systems, the number of peaks in the O *K*-edge region that are due to the hybridization of O 2*p* with transition metal 3*d* orbitals appears to be correlated with the number of nonequivalent oxygen sites in the structure.[70–76] These sites have different distances to the transition metal, and their orbitals hybridize differently with the transition metal 3*d* orbitals, giving rise to multiple peaks at different energies. In the case of bulk $SrCuO_{2.5}$, the average copper-oxygen distance is ~1.866 Å in the *c* (out-of-plane) direction, while it is ~1.917 Å in the *a*/*b* (in-plane) directions, suggesting that Cu 3*d*– O 2*p* hybridization will be different for different oxygen sites.

Second, the appearance of a low-energy feature in the O *K* edge is consistent with x-ray absorption studies of other hole-doped cuprates.[4,58,60,62,63,68] The intensity of this low-energy peak was observed to increase as a function of hole doping. Considering that in our case, both structural and electronic changes occur between $SrCuO_2$ and $SrCuO_{2+\delta}$, a one-to-one comparison of the O *K*-edge region with other hole-doped cuprates like $La_{2-x}Sr_xCuO_4$ is more difficult. However, we can confirm that the $SrCuO_{2+\delta}$ structure is hole doped using field-effect experiments using the $SrTiO_3$ substrate as the gate dielectric, as shown in the supplementary material Fig. S6.

Doping in the infinite-layer cuprate systems can lead to drastic changes in their resistivity and even to superconductivity. Figure 6(a) shows the behavior of the resistivity of different studied films as a function of temperature, revealing the sensitivity of this compound to the oxidizing growth conditions. In the plot, the infinite-layer $SrCuO_2$ film deposited in pure oxygen has a resistivity of the order of 1×10^4 $\mu\Omega$ cm at room temperature and exhibits insulating behavior as a function of temperature, reaching values of 1×10^7 $\mu\Omega$ cm at low temperatures.

As additional oxygen is introduced into the structure and the transformation to the high *c*-axis $SrCuO_{2+\delta}$ phase occurs, the resistivity decreases very drastically and reaches values lower than 1 mΩ cm at room temperature. This decrease in resistivity does not come from a drastic change in sample topography, as the surface roughness of the films of Fig. 6(a) does not change significantly, as shown in the supplementary material Fig. S7. A similar decrease in resistivity has been observed in high *c*-axis $SrCuO_{2+\delta}$ thin films that have been plasma-annealed,[38] cooled in atomic oxygen[40] or ozone.[41] Nevertheless, superconductivity is not observed in the $SrCuO_{2+\delta}$ system, probably due to the very high level of doping (that goes beyond the superconducting dome of the cuprates[2]), as well as the absence of continuous CuO_2 planes.

For $SrCuO_{2+\delta}$ films in the high *c*-axis phase, we find a variation in the temperature dependence of the resistivity that is correlated with the value of the out-of-plane lattice parameter of each film. Figures 6(b) and 6(c) show the resistivity behavior of two $SrCuO_{2+\delta}$ thin films with $c = 3.63$ Å and $c = 3.67$ Å, respectively: the film with the lower lattice parameter exhibits metallic behavior down to ~100 K, with an upturn at lower temperatures; in contrast, the film with the larger lattice parameter exhibits semiconducting/insulating behavior at all temperatures below 300 K. We note that, while it is possible that differing degrees of disorder could impact the

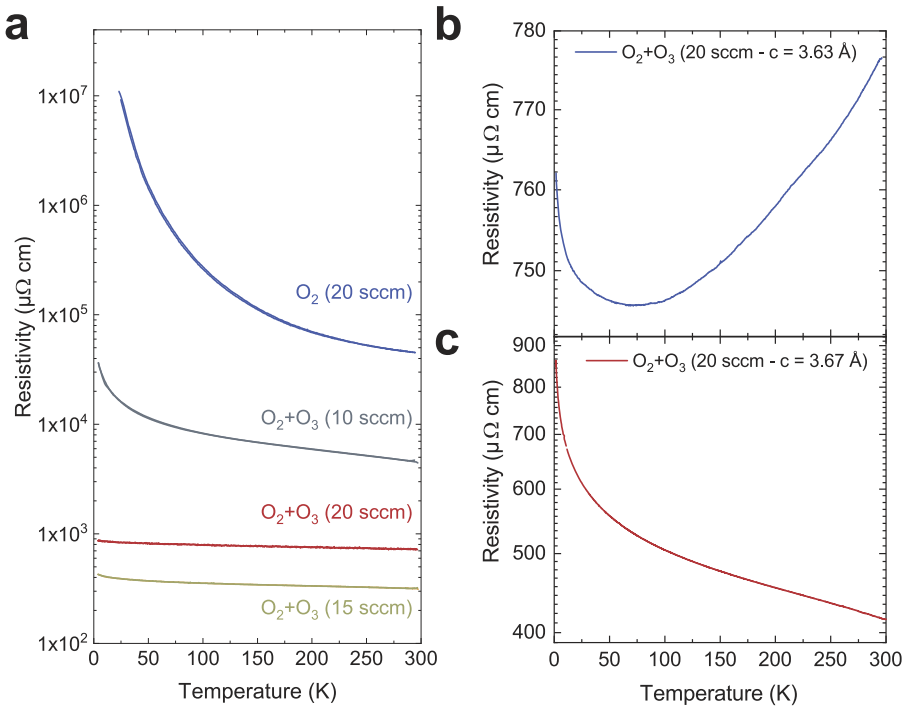

FIG. 6. (a) Resistivity as a function of temperature of a series of $SrCuO_{2+\delta}$ films deposited under varying oxidizing growth conditions. Top curve (in blue): Film deposited in pure oxygen. Bottom curves: Films deposited with an ozone/oxygen ratio of ~5%, where the oxidizing power is progressively increased by increasing the flow rate from 10 to 20 sccm. A clear decrease in resistivity is observed as the oxygen content of the films is increased, consistent with doping. (b) and (c) Resistivity as a function of temperature for two films deposited under highly oxidizing growth conditions, with out-of-plane lattice parameters of 3.63 and 3.67 Å, respectively, showing that the film with the lower lattice parameter is metallic down to ~100 K.

behavior of the resistivity, x-ray diffraction measurements reveal no significant difference in the quality of the two films.

This is the first indication that the resistivity is highly dependent on the precise oxygen content of the structure, as in conventional hole-doped cuprates.[19] Among the high *c*-axis structure thin films, lower out-of-plane lattice parameters signify a smaller number of oxygen atoms in the SrO_x planes and, therefore, a nominal copper valence smaller than 3+.[2] In contrast, films with larger out-of-plane lattice parameters have a higher oxygen content and are closer to $SrCuO_{2.5}$, a structure with a nominal Cu 3+ valence.

IV. CONCLUSIONS

In summary, we have used ozone-assisted pulsed laser deposition to fabricate high-quality $SrCuO_{2+\delta}$ thin films on $SrTiO_3$ substrates. At low oxidizing power (deposition using pure oxygen), the infinite-layer $SrCuO_2$ structure is stabilized. As the oxidizing power is increased, a different phase with an elongated *c* axis appears ($SrCuO_{2+\delta}$), with a macroscopic $SrCuO_2$ vs $SrCuO_{2+\delta}$ phase fraction that can be varied by controlling the O_3/O_2 flow. Planar-view scanning transmission electron microscopy measurements have shown that the $SrCuO_{2+\delta}$ thin films are characterized by regions of an expanded in-plane lattice parameter, appearing due to the ordering of oxygen vacancies along either the [100] or the [010] direction when δ is smaller than 0.5. X-ray absorption spectroscopy measurements around the Cu $L_{2,3}$ and O *K* edges indicate that the high *c*-axis phase has a more isotropic Cu orbital configuration and is hole doped compared to the infinite-layer $SrCuO_2$ phase. The resistivity of the $SrCuO_{2+\delta}$ thin films was measured as a function of temperature, revealing a dramatic decrease with hole doping, with a magnitude that depends on the precise oxygen content of the structure.

Our work provides useful insight concerning the role of oxygen and the way it can be accommodated in epitaxially strained infinite-layer cuprate structures, uncovering a new way in which these $SrCuO_{2+\delta}$ thin films accommodate oxygen vacancies compared to stoichiometric $SrCuO_{2.5}$ structures. We believe that these results will contribute to further understanding of the behavior of infinite-layer cuprate thin films and will also inspire further studies on the use of ozone to control the precise oxygen content and Cu coordination in these systems.

SUPPLEMENTARY MATERIAL

See the supplementary material for more information on the growth conditions of $SrCuO_2$ thin films, the other possible structures of $SrCuO_{2+\delta}$, annealing experiments of the $SrCuO_{2+\delta}$ phase, x-ray linear dichroism at the O *K* edge, fitting of the Cu L_3 edge, gating experiments on $SrCuO_{2+\delta}$, and atomic force microscopy characterization of the thin films.

ACKNOWLEDGMENTS

We thank Marco Lopes for technical support, Jérémy Bettex for the preparation of the STEM specimen, Giuseppe Balestrino and Daniele Di Castro for their advice concerning the use of ozone during sample growth, and Atsuto Seko for providing the calculated structure files of Ref. 45. We also acknowledge Philippe Ghosez, Yajun Zhang, Alexandre Gloter, and Marc Gabay for fruitful discussions. This work was supported by the Swiss National Science Foundation—Division II (Grant No. 200020_179155) and by the European Research Council under the European Union Seventh Framework Programme, Grant No. FP7/2007–2013 and ERC Grant Agreement No. 319286 (Q-MAC). We acknowledge the ALBA synchrotron facility and the BL29 beamline staff for support during the x-ray absorption spectroscopy experiment. M.G. and G.D.L. acknowledge support by the Swiss National Science Foundation under Grant No. PP00P2_170564.

AUTHOR DECLARATIONS

Conflict of Interest

The authors have no conflicts to disclose.

Author Contributions

Marios Hadjimichael and Adrien Waelchi contributed equally to this work.

Marios Hadjimichael: Conceptualization (lead); Formal analysis (lead); Investigation (equal); Methodology (equal); Writing – original draft (equal); Writing – review & editing (equal). **Adrien Waelchli**: Formal analysis (equal); Investigation (equal); Methodology (equal); Writing – original draft (supporting); Writing – review & editing (equal). **Bernat Mundet**: Formal analysis (supporting); Investigation (supporting); Methodology (supporting). **Siobhan McKeown Walker**: Formal analysis (supporting); Investigation (supporting). **Gabriele De Luca**: Formal analysis (supporting); Investigation (supporting); Methodology (supporting); Writing – original draft (supporting); Writing – review & editing (supporting). **Javier Herrero-Martín**: Investigation (supporting); Methodology (supporting); Writing – original draft (supporting); Writing – review & editing (supporting). **Marta Gibert**: Formal analysis (supporting); Investigation (supporting); Methodology (supporting); Writing – original draft (supporting); Writing – review & editing (supporting). **Stefano Gariglio**: Conceptualization (supporting); Formal analysis (equal); Funding acquisition (supporting); Investigation (supporting); Methodology (supporting); Project administration (supporting); Resources (supporting); Writing – original draft (equal); Writing – review & editing (equal). **Jean-Marc Triscone**: Conceptualization (supporting); Funding acquisition (lead); Project administration (lead); Resources (lead); Supervision (lead).

DATA AVAILABILITY

The data that support the findings of this study are openly available in the Yareta repository at https://doi.org/10/gqx6bd.

REFERENCES

[1] J. G. Bednorz and K. A. Müller, Z. Phys. B: Condens. Matter **64**, 189 (1986).
[2] B. Keimer, S. A. Kivelson, M. R. Norman, S. Uchida, and J. Zaanen, Nature **518**, 179 (2015).
[3] T. Siegrist, S. M. Zahurak, D. W. Murphy, and R. S. Roth, Nature **334**, 231 (1988).
[4] W. M. Li, J. F. Zhao, L. P. Cao, Z. Hu, Q. Z. Huang, X. C. Wang, Y. Liu, G. Q. Zhao, J. Zhang, Q. Q. Liu, R. Z. Yu, Y. W. Long, H. Wu, H. J. Lin, C. T. Chen,

Z. Li, Z. Z. Gong, Z. Guguchia, J. S. Kim, G. R. Stewart, Y. J. Uemura, S. Uchida, and C. Q. Jin, Proc. Natl. Acad. Sci. U. S. A. **116**, 12156 (2019).
[5]D. Li, K. Lee, B. Y. Wang, M. Osada, S. Crossley, H. R. Lee, Y. Cui, Y. Hikita, and H. Y. Hwang, Nature **572**, 624 (2019).
[6]D. Li, B. Y. Wang, K. Lee, S. P. Harvey, M. Osada, B. H. Goodge, L. F. Kourkoutis, and H. Y. Hwang, Phys. Rev. Lett. **125**, 027001 (2020).
[7]M. Osada, B. Y. Wang, B. H. Goodge, K. Lee, H. Yoon, K. Sakuma, D. Li, M. Miura, L. F. Kourkoutis, and H. Y. Hwang, Nano Lett. **20**, 5735 (2020).
[8]M. Osada, B. Y. Wang, K. Lee, D. Li, and H. Y. Hwang, Phys. Rev. Mater. **4**, 121801(R) (2020).
[9]S. Zeng, C. S. Tang, X. Yin, C. Li, M. Li, Z. Huang, J. Hu, W. Liu, G. J. Omar, H. Jani, Z. S. Lim, K. Han, D. Wan, P. Yang, S. J. Pennycook, A. T. S. Wee, and A. Ariando, Phys. Rev. Lett. **125**, 147003 (2020).
[10]M. Osada, B. Y. Wang, B. H. Goodge, S. P. Harvey, K. Lee, D. Li, L. F. Kourkoutis, and H. Y. Hwang, Adv. Mater. **33**, 2104083 (2021).
[11]M. G. Smith, A. Manthiram, J. Zhou, J. B. Goodenough, and J. T. Markert, Nature **351**, 549 (1991).
[12]G. Er, Y. Miyamoto, F. Kanamaru, and S. Kikkawa, Physica C **181**, 206 (1991).
[13]M. Azuma, Z. Hiroi, M. Takano, Y. Bando, and Y. Takeda, Nature **356**, 775 (1992).
[14]M. Kanai, T. Kawai, and S. Kawai, Appl. Phys. Lett. **58**, 771 (1991).
[15]N. Terada, G. Zouganelis, M. Jo, M. Hirabayashi, K. Kaneko, and H. Ihara, Physica C **185-189**, 2019 (1991).
[16]D. P. Norton, B. C. Chakoumakos, J. D. Budai, and D. H. Lowndes, Appl. Phys. Lett. **62**, 1679 (1993).
[17]Y. Tokura, H. Takagi, and S. Uchida, Nature **337**, 345 (1989).
[18]N. P. Armitage, P. Fournier, and R. L. Greene, Rev. Mod. Phys. **82**, 2421 (2010).
[19]C. W. Chu, L. Z. Deng, and B. Lv, Physica C **514**, 290 (2015).
[20]D. P. Norton, B. C. Chakoumakos, J. D. Budai, D. H. Lowndes, B. C. Sales, J. R. Thompson, and D. K. Christen, Science **265**, 2074 (1994).
[21]D. P. Norton, B. C. Chakoumakos, J. D. Budai, J. R. Thompson, and D. H. Lowndes, J. Supercond. **8**, 519 (1995).
[22]X. Li, T. Kawai, and S. Kawai, Jpn. J. Appl. Phys. **33**, L18 (1994).
[23]G. Balestrino, C. Ferdeghini, S. Gariglio, D. Marrè, P. G. Medaglia, G. Petrocelli, and A. S. Siri, Solid State Commun. **108**, 499 (1998).
[24]D. Di Castro, M. Salvato, A. Tebano, D. Innocenti, C. Aruta, W. Prellier, O. I. Lebedev, I. Ottaviani, N. B. Brookes, M. Minola, M. Moretti Sala, C. Mazzoli, P. G. Medaglia, G. Ghiringhelli, L. Braicovich, M. Cirillo, and G. Balestrino, Phys. Rev. B **86**, 134524 (2012).
[25]D. Di Castro, C. Cantoni, F. Ridolfi, C. Aruta, A. Tebano, N. Yang, and G. Balestrino, Phys. Rev. Lett. **115**, 147001 (2015).
[26]L. Jones, H. Yang, T. J. Pennycook, M. S. J. Marshall, S. Van Aert, N. D. Browning, M. R. Castell, and P. D. Nellist, Adv. Struct. Chem. Imaging **1**, 8 (2015).
[27]M. Nord, P. E. Vullum, I. MacLaren, T. Tybell, and R. Holmestad, Adv. Struct. Chem. Imaging **3**, 9 (2017).
[28]A. Barla, J. Nicolás, D. Cocco, S. M. Valvidares, J. Herrero-Martín, P. Gargiani, J. Moldes, C. Ruget, E. Pellegrin, and S. Ferrer, J. Synchrotron Radiat. **23**, 1507 (2016).
[29]Y. Matsushita, Y. Oyama, M. Hasegawa, and H. Takei, J. Solid State Chem. **114**, 289 (1994).
[30]C. N. Mihailescu, I. Pasuk, G. I. Athanasopoulos, C. Luculescu, M. Socol, R. Saint-Martin, A. Revcolevschi, and J. Giapintzakis, Appl. Surf. Sci. **278**, 132 (2013).
[31]C. N. Mihailescu, I. Pasuk, M. Straticiuc, C. R. Nita, D. Pantelica, and J. Giapintzakis, Appl. Surf. Sci. **320**, 852 (2014).
[32]Z. Zhong, G. Koster, and P. J. Kelly, Phys. Rev. B **85**, 121411 (2012).
[33]D. Samal, H. Tan, H. Molegraaf, B. Kuiper, W. Siemons, S. Bals, J. Verbeeck, G. Van Tendeloo, Y. Takamura, E. Arenholz, C. A. Jenkins, G. Rijnders, and G. Koster, Phys. Rev. Lett. **111**, 096102 (2013).
[34]Z. Liao, E. Skoropata, J. W. Freeland, E.-J. Guo, R. Desautels, X. Gao, C. Sohn, A. Rastogi, T. Z. Ward, T. Zou, T. Charlton, M. R. Fitzsimmons, and H. N. Lee, Nat. Commun. **10**, 589 (2019).
[35]C. L. Teske and H. Müller-Buschbaum, Z. Anorg. Allg. Chem. **371**, 325 (1969).
[36]Z. Hiroi, M. Takano, M. Azuma, and Y. Takeda, Nature **364**, 315 (1993).
[37]Y. Shimakawa, J. D. Jorgensen, J. F. Mitchell, B. A. Hunter, H. Shaked, D. G. Hinks, R. L. Hitterman, Z. Hiroi, and M. Takano, Physica C **228**, 73 (1994).
[38]H. Yakabe, A. Kume, J. G. Wen, M. Kosuge, Y. Shiohara, and N. Koshizuka, Physica C **232**, 371 (1994).
[39]J. G. Wen, H. Yakabe, A. Kume, Y. Shiohara, N. Koshizuka, and S. Tanaka, Physica C **228**, 279 (1994).
[40]A. Gupta, B. W. Hussey, T. M. Shaw, A. M. Guloy, M. Y. Chern, R. F. Saraf, and B. A. Scott, J. Solid State Chem. **112**, 113 (1994).
[41]A. Tsukamoto, J. G. Wen, K. Nakanishi, and K. Tanabe, Physica C **292**, 17 (1997).
[42]H. Adachi, T. Satoh, Y. Ichikawa, K. Setsune, and K. Wasa, Physica C **196**, 14 (1992).
[43]V. Leca, D. H. A. Blank, G. Rijnders, S. Bals, and G. Van Tendeloo, Appl. Phys. Lett. **89**, 092504 (2006).
[44]J. Tomaschko, V. Leca, T. Selistrovski, S. Diebold, J. Jochum, R. Kleiner, and D. Koelle, Phys. Rev. B **85**, 024519 (2012).
[45]A. Seko and S. Ishiwata, Phys. Rev. B **101**, 134101 (2020).
[46]X. Zhou, F. Wu, B. Yin, W. Liu, C. Dong, J. Li, W. Zhu, S. Jia, Y. Yao, and Z. Zhao, Physica C **233**, 311 (1994).
[47]B.-H. Chen, D. Walker, B. A. Scott, and D. B. Mitzi, J. Solid State Chem. **121**, 498 (1996).
[48]K. R. Poeppelmeier, M. E. Leonowicz, J. C. Scanlon, J. M. Longo, and W. B. Yelon, J. Solid State Chem. **45**, 71 (1982).
[49]J. F. Bringley, B. A. Scott, S. J. La Placa, R. F. Boehme, T. M. Shaw, M. W. McElfresh, S. S. Trail, and D. E. Cox, Nature **347**, 263 (1990).
[50]D. O. Klenov, W. Donner, B. Foran, and S. Stemmer, Appl. Phys. Lett. **82**, 3427 (2003).
[51]Y.-M. Kim, J. He, M. D. Biegalski, H. Ambaye, V. Lauter, H. M. Christen, S. T. Pantelides, S. J. Pennycook, S. V. Kalinin, and A. Y. Borisevich, Nat. Mater. **11**, 888 (2012).
[52]N. Biškup, J. Salafranca, V. Mehta, M. P. Oxley, Y. Suzuki, S. J. Pennycook, S. T. Pantelides, and M. Varela, Phys. Rev. Lett. **112**, 087202 (2014).
[53]J. D. Ferguson, Y. Kim, L. F. Kourkoutis, A. Vodnick, A. R. Woll, D. A. Muller, and J. D. Brock, Adv. Mater. **23**, 1226 (2011).
[54]K. Hirai, D. Kan, R. Aso, N. Ichikawa, H. Kurata, and Y. Shimakawa, J. Appl. Phys. **114**, 053514 (2013).
[55]T. G. Parsons, H. D'Hondt, J. Hadermann, and M. A. Hayward, Chem. Mater. **21**, 5527 (2009).
[56]D. D. Sarma, O. Strebel, C. T. Simmons, U. Neukirch, G. Kaindl, R. Hoppe, and H. P. Müller, Phys. Rev. B **37**, 9784 (1988).
[57]M. Grioni, J. B. Goedkoop, R. Schoorl, F. M. F. de Groot, J. C. Fuggle, F. Schäfers, E. E. Koch, G. Rossi, J.-M. Esteva, and R. C. Karnatak, Phys. Rev. B **39**, 1541 (1989).
[58]C. T. Chen, F. Sette, Y. Ma, M. S. Hybertsen, E. B. Stechel, W. M. C. Foulkes, M. Schulter, S.-W. Cheong, A. S. Cooper, L. W. Rupp, B. Batlogg, Y. L. Soo, Z. H. Ming, A. Krol, and Y. H. Kao, Phys. Rev. Lett. **66**, 104 (1991).
[59]M. Ronay, A. Santoni, A. G. Schrott, L. J. Terminello, S. P. Kowalczyk, and F. J. Himpsel, Solid State Commun. **77**, 699 (1991).
[60]C. T. Chen, L. H. Tjeng, J. Kwo, H. L. Kao, P. Rudolf, F. Sette, and R. M. Fleming, Phys. Rev. Lett. **68**, 2543 (1992).
[61]A. Q. Pham, F. Studer, N. Merrien, A. Maignan, C. Michel, and B. Raveau, Phys. Rev. B **48**, 1249 (1993).
[62]J. Fink, N. Nücker, E. Pellegrin, H. Romberg, M. Alexander, and M. Knupfer, J. Electron Spectrosc. Relat. Phenom. **66**, 395 (1994).
[63]E. Pellegrin, N. Nücker, J. Fink, S. L. Molodtsov, A. Gutiérrez, E. Navas, O. Strebel, Z. Hu, M. Domke, G. Kaindl, S. Uchida, Y. Nakamura, J. Markl, M. Klauda, G. Saemann-Ischenko, A. Krol, J. L. Peng, Z. Y. Li, and R. L. Greene, Phys. Rev. B **47**, 3354 (1993).
[64]C. Aruta, G. Ghiringhelli, C. Dallera, F. Fracassi, P. G. Medaglia, A. Tebano, N. B. Brookes, L. Braicovich, and G. Balestrino, Phys. Rev. B **78**, 205120 (2008).
[65]D. I. Khomskii, *Transition Metal Compounds* (Cambridge University Press, 2014), pp. 1–485.

[66] A. Bianconi, A. C. Castellano, M. De Santis, P. Rudolf, P. Lagarde, A. M. Flank, and A. Marcelli, Solid State Commun. **63**, 1009 (1987).
[67] D. Meyers, S. Mukherjee, J.-G. Cheng, S. Middey, J.-S. Zhou, J. B. Goodenough, B. A. Gray, J. W. Freeland, T. Saha-Dasgupta, and J. Chakhalian, Sci. Rep. **3**, 1834 (2013).
[68] D. Choudhury, P. Rivero, D. Meyers, X. Liu, Y. Cao, S. Middey, M. J. Whitaker, S. Barraza-Lopez, J. W. Freeland, M. Greenblatt, and J. Chakhalian, Phys. Rev. B **92**, 201108 (2015).
[69] P. Ghigna, G. Spinolo, G. Flor, and N. Morgante, Phys. Rev. B **57**, 13426 (1998).
[70] M. Merz, N. Nücker, P. Schweiss, S. Schuppler, C. T. Chen, V. Chakarian, J. Freeland, Y. U. Idzerda, M. Kläser, G. Müller-Vogt, and T. Wolf, Phys. Rev. Lett. **80**, 5192 (1998).
[71] G. P. Zhang, G. T. Woods, E. L. Shirley, T. A. Callcott, L. Lin, G. S. Chang, B. C. Sales, D. Mandrus, and J. He, Phys. Rev. B **65**, 165107 (2002).
[72] M. Abbate, G. Zampieri, F. Prado, A. Caneiro, J. M. Gonzalez-Calbet, and M. Vallet-Regi, Phys. Rev. B **65**, 155101 (2002).
[73] S. Valencia, A. Gaupp, W. Gudat, L. Abad, L. Balcells, B. Martínez, and V. Laukhin, Appl. Phys. Lett. **89**, 172512 (2006).
[74] Y. T. Tsai, W. J. Chang, S. W. Huang, J.-Y. Lin, J. Y. Lee, J. M. Chen, K. H. Wu, T. M. Uen, Y. S. Gou, and J. Y. Juang, Physica B **404**, 1404 (2009).
[75] A. Chassé, S. Borek, K.-M. Schindler, M. Trautmann, M. Huth, F. Steudel, L. Makhova, J. Gräfe, and R. Denecke, Phys. Rev. B **84**, 195135 (2011).
[76] F. Frati, M. O. J. Y. Hunault, and F. M. F. de Groot, Chem. Rev. **120**, 4056 (2020).